

## Electronic Origin of Non-Zone-Center Phonon Condensation: Octahedral Rotation as a Case Study

Suguru Yoshida<sup>1</sup>,\* Hirofumi Akamatsu<sup>1</sup>, and Katsuro Hayashi<sup>1</sup>

*Department of Applied Chemistry, Kyushu University, Motoooka, Fukuoka 819-0395, Japan*

 (Received 14 May 2021; revised 17 September 2021; accepted 15 October 2021; published 19 November 2021)

Unstable zone-boundary phonon modes drive atomic displacements linked to a rich array of properties. Yet, the electronic origin of the instability remains to be clearly explained. In this Letter, we propose that bonding interaction between Bloch states belonging to different wave vectors leads to such instability via the pseudo- or second-order Jahn–Teller effect. Our first-principles calculations and representation theory-based analyses show that rotations of anion coordinated octahedra, an archetypal example of zone-boundary phonon condensations, are induced by this bonding mechanism. The proposed mechanism is universal to any non-zone-center phonon condensations and could offer a general approach to understanding the origin of structural phase transitions in crystals.

DOI: [10.1103/PhysRevLett.127.215701](https://doi.org/10.1103/PhysRevLett.127.215701)

Collective changes in atom positions often have drastic influences on the physical properties of solids. Examples include polar atomic displacements emerging from the condensation of a transverse optic phonon at the Brillouin-zone center (wave vector  $\mathbf{q} = 0$ ) [1] through which the crystal acquires a ferroelectric nature. Displacements with finite wave vectors can also lead to functionalities inaccessible by zone-center phonon condensations. In particular, rotations of rigid polyhedral units, which arise from the condensation of phonon modes at the Brillouin-zone boundary, have recently attracted attention because of their strong coupling to magnetic [2–4], electric [5–7], thermal [8–10], conducting [11,12], and emitting [13] properties as well as their utility for realizing cross-coupled multiferroics [14–16].

Key electronic features that favor the zero- $\mathbf{q}$  displacements have been unveiled over the past few decades [17–20], facilitating the design of new polar materials. In contrast, up to now, available information on the mechanism driving nonzero- $\mathbf{q}$  displacements has been almost limited to the classical information [21]. For example, octahedral rotations (ORs) in perovskitelike compounds have long been attributed to ionic size mismatch, i.e., a coordination preference of *A*-site cations [22]. Even though this explanation is useful for foreseeing whether a given material will exhibit ORs or not, it lacks the ability to predict the rotational pattern, which is actually sensitive to electron correlations as reported in Ref. [23]. A deep insight would be highly desirable for harnessing nonzero- $\mathbf{q}$  displacements and paving a promising route to manipulate the material's functionality.

This Letter proposes a quantum-mechanical and group-theoretical framework for explaining the driving force for nonzero- $\mathbf{q}$  displacements in terms of electronic band

structures. We employ an approach adopting a second-order Jahn–Teller (SOJT) effect [24], which has been successfully applied with point-group analyses to describe the electronic origin of zero- $\mathbf{q}$  displacements [17] and molecular deformations [25,26]. Although previous studies have discussed mechanisms behind some zone-boundary distortion from the perspective of electron-lattice interactions [27–29], there are, to our knowledge, no reports offering a general approach applicable to any arbitrary displacement in a material. Here, we utilize space-group representation theory to treat translational symmetry breaking by nonzero- $\mathbf{q}$  displacements and consequently demonstrate that the SOJT-based approach can go beyond zero- $\mathbf{q}$  displacements while preserving its general applicability. We apply our method to *A*-site-empty perovskites, i.e.,  $\text{ReO}_3$ -type  $\text{BX}_3$  compounds, and reveal why the octahedra rotate even without *A*-site cations. A study on  $\text{ABX}_3$  perovskites is given in the Supplemental Material [30]. Our findings highlight that bonding interactions significantly contribute to the driving mechanism of the ORs, which was believed to be genuinely geometric.

We start by reviewing perturbative treatments of the SOJT effect [48,49], which enables deriving selection rules that underlie our discussion. The total energy ( $E$ ) of a system with Hamiltonian  $\mathcal{H}$  can be expanded in terms of normal coordinate ( $Q$ ) about the reference phase:

$$E = E_0 + \langle 0 | \mathcal{H}^{(1)} | 0 \rangle Q + \frac{1}{2} \left[ \langle 0 | \mathcal{H}^{(2)} | 0 \rangle - 2 \sum_n \frac{|\langle 0 | \mathcal{H}^{(1)} | n \rangle|^2}{E_n - E_0} \right] Q^2 + \dots, \quad (1)$$

with

$$\mathcal{H}^{(1)} = \left. \frac{\partial \mathcal{H}}{\partial Q} \right|_{Q=0}, \quad \text{and} \quad \mathcal{H}^{(2)} = \left. \frac{\partial^2 \mathcal{H}}{\partial Q^2} \right|_{Q=0}. \quad (2)$$

$E_0$  and  $E_n$  refer to the energy of the ground state  $|0\rangle$  and excited state  $|n\rangle$ , respectively, both of which are eigenstates of the Hamiltonian for the reference phase with the space group  $\mathcal{G}$ . Let  $|0\rangle$  and  $|n\rangle$  transform as irreducible representations (irreps)  $\Phi_0$  and  $\Phi_n$  of  $\mathcal{G}$ , respectively. Note that  $\mathcal{H}^{(1)}$  transforms as the same irrep as  $Q$  and the corresponding phonon mode [50]; it will be denoted by  $\Phi_P$ . Of the quadratic terms in  $Q$ , the first one is positive in an approximation in which the wave functions are frozen, favoring the structure with  $Q = 0$ . On the other hand, the second term  $-2 \sum_n \{ |\langle 0 | \mathcal{H}^{(1)} | n \rangle|^2 / [E_n - E_0] \}$  is negative unless the matrix element  $\langle 0 | \mathcal{H}^{(1)} | n \rangle$  is forced to vanish by symmetry. The following two conditions should be fulfilled for the magnitude of the second term to be larger than that of the first one so that the system undergoes the energy-lowering structural distortion, which is known as the strong SOJT effect [26]. First, the direct product  $\Phi_0 \otimes \Phi_P \otimes \Phi_n$  should contain the totally symmetric representation of  $\mathcal{G}$  or equivalently  $\Phi_0 \otimes \Phi_n$  should contain  $\Phi_P$  to attain a non-zero value for  $\langle 0 | \mathcal{H}^{(1)} | n \rangle$  [51], representing the mixing of two electronic states in response to displacement perturbation. Second, the energy gap  $E_n - E_0$  in the denominator should be small. Therefore, a distortion occurs if the corresponding phonon mode is symmetry allowed to invoke mixing of the ground and low-lying excited states.

The mixing of electronic states is referred to as covalent bond formations in the low-symmetry phase [26]. Let us consider a polar displacement ( $\mathbf{q} = 0$ ) in BaTiO<sub>3</sub> [Fig. 1(a)]. In the high-symmetry  $Pm\bar{3}m$  structure, the valence band (VB, dominated by O  $2p$ ) and conduction band (CB, dominated by Ti  $3d-t_{2g}$ ) have different symmetries belonging to distinct irreps,  $\Gamma_4^-$  and  $\Gamma_5^+$ , respectively, whereby the overlap of the two wave functions is forbidden (step 1).

Once the Ti nuclei shift in a polar fashion ( $\Gamma_4^-$ ), the crystal symmetry lowers from  $Pm\bar{3}m$  to  $P4mm$ , and concomitantly the degeneracies of the two electronic states are lifted (step 2). How they split is defined by compatibility relations [51]. Two-thirds of O  $2p$  and Ti  $3d-t_{2g}$  states now transform as the same irrep  $[\Gamma_5]_{P4mm}$  [52] so that bonding and antibonding states appear through electronic relaxation, i.e., orbital mixing (step 3). Given the appropriate electron count, the bonding and nonbonding states accommodate the electrons to stabilize the low-symmetry configuration. This is a chemistry explanation for the SOJT effect.

The perturbative and symmetry arguments have no restriction on the  $\mathbf{q}$  value, implying that this framework should also provide insights into the origin of nonzero- $\mathbf{q}$  displacements. However, symmetry forbids any  $\Gamma$ - $\Gamma$  bond formation—like that shown in Fig. 1(a)—stemming from displacements with finite  $\mathbf{q}$ . Although this fact seems to rule out the possibility that the bonding mechanism is at play, nonzero- $\mathbf{q}$  displacements can give rise to, as we demonstrate later, mixing between two states with different  $\mathbf{k}$ -vectors from each other and thus arise through the SOJT mechanism.

We utilize the band structure to treat all Bloch states in a crystal, not just those at the  $\Gamma$  point represented in the energy diagram. Figure 1(b) illustrates how a displacement ( $\mathbf{q} = (\pi/a)$ ) results in the mixing of a VB state at  $\mathbf{k} = (\pi/a)$  with a CB state at  $\mathbf{k} = 0$ , where  $a$  is the lattice constant of the reference phase. The VB state cannot interact with the CB state in the reference configuration because of the discrepancy in  $\mathbf{k}$ -vectors (step 1). Once the crystal experiences a distorting perturbation with the periodicity of  $2a$ , the unit cell doubles while folding the electronic bands into the halved first Brillouin zone (step 2). This band folding places the VB and CB states at the identical  $\mathbf{k}$ -point, accepting the bond formation required to stabilize the distorted configuration. The relevant VB and CB states are most commonly the VB maximum (VBM) and CB minimum (CBM), respectively, in analogy with molecular deformations [30]. Note that the  $\mathbf{k}$ -matching between two states under perturbation is merely a necessary condition for the states to mix; namely, we must further examine whether the direct product  $\Phi_0 \otimes \Phi_P \otimes \Phi_n$  of the space-group irreps comprises the totally symmetric representation or not to make sure that the distorting perturbation is symmetry allowed to induce bond formation (step 3).

By choosing ORs in ReO<sub>3</sub>-type  $BX_3$  compounds as a case study, we illustrate how the SOJT-based approach integrated with space-group representation theory explains the emergence of nonzero- $\mathbf{q}$  displacements. It is believed that, in perovskites, octahedra rotate to optimize the coordination environment for A-site cations otherwise underbonded. However, ReO<sub>3</sub>-type compounds generally exhibit ORs rather than remain the aristotype  $Pm\bar{3}m$  structure despite no A-site cations; a majority of fluoride (pnictide) members crystallize in  $R\bar{3}c$  ( $Im\bar{3}$ ) structures

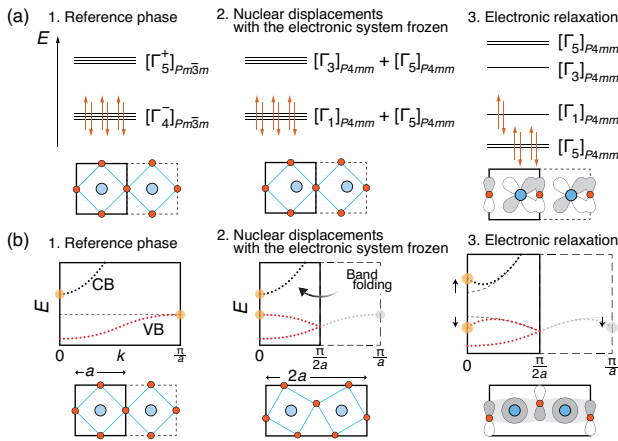


FIG. 1. Step-by-step illustration of the SOJT mechanism driving (a) zone-center ( $\mathbf{q} = 0$ ) and (b) zone-boundary ( $\mathbf{q} = (\pi/a)$ ) phonon condensation.

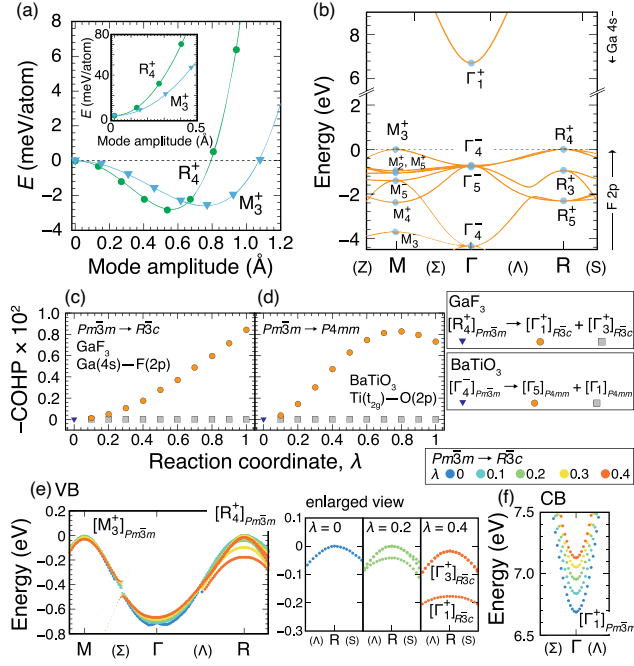


FIG. 2. (a) Total energy and Madelung energy (shown in the inset) of  $\text{GaF}_3$  as a function of the amplitude of out-of-phase ( $R_4^+$ ) and in-phase ( $M_3^+$ ) OR modes. (b) Electronic band structure for  $\text{GaF}_3$  adopting  $Pm\bar{3}m$  symmetry with the irrep labels. The band-resolved  $-\text{COHPs}$  for the (c)  $R_4^+$  VB states of  $\text{GaF}_3$  and (d)  $\Gamma_4^-$  VB states of  $\text{BaTiO}_3$  as a function of reaction coordinate  $\lambda$ . The legend on the right explains how the VB states split as  $\lambda$  rises from zero. Band structures of  $\text{GaF}_3$  in the energy region near the (e) VBM and (f) CBM as a function of  $\lambda$ , where all the bands including those of  $R\bar{3}c$  structures ( $\lambda \neq 0$ ) are drawn along the high-symmetry path of the  $Pm\bar{3}m$  structure ( $\lambda = 0$ ) via band unfolding.

involving out-of-phase  $a^-a^-a^-$ -type (in-phase  $a^+a^+a^+$ -type) ORs [53]. Hereafter, we also address this question as to what drives ORs. First-principles calculations were performed for  $\text{ReO}_3$ -type compounds— $\text{GaF}_3$ ,  $\text{RhF}_3$ ,  $\text{AlH}_3$ ,  $\text{ReO}_3$ , and  $\text{RhP}_3$ —and perovskite  $\text{BaTiO}_3$  using the projector augmented-wave method [54,55] and the HSE06 hybrid functional [56–58] as implemented in VASP code [59–62]. Details are given in the Supplemental Material [30].

We first focus on  $\text{GaF}_3$ , whose  $R\bar{3}c$  structure has been experimentally identified [63]. Figure 2(a) shows that substantial energy gains relative to the  $Pm\bar{3}m$  configuration are observed for  $a^-a^-a^-$ -type and  $a^+a^+a^+$ -type OR modes transforming as the irrep  $R_4^+$  and  $M_3^+$ , respectively. It means that the ORs are energetically favorable within density functional theory. On the other hand, ORs are unfavorable at the level of an electrostatic model, as evident from the inset of Fig. 2(a). This qualitative disagreement corroborates that nonclassical behavior of electrons excluded in Madelung energy calculations is vital for understanding stabilization mechanisms behind ORs.

We consider how the  $R\bar{3}c$  phase appears through the SOJT mechanism, i.e., the case of  $\Phi_P = R_4^+$ . Discussions on the in-phase  $Im\bar{3}$  phase and its difference from the  $R\bar{3}c$  phase regarding orbital interactions are given in the Supplemental Material [30]. The calculated electronic band structure [Fig. 2(b)] shows that the VBM (CBM) of  $\text{GaF}_3$  with the  $Pm\bar{3}m$  structure is at R ( $\Gamma$ ) point and transforms like the irrep  $R_4^+$  ( $\Gamma_1^+$ ) of  $Pm\bar{3}m$ . Using the irreps of the VBM, CBM, and considered distortion mode, we calculate the direct product  $\Phi_0 \otimes \Phi_P \otimes \Phi_n$ :

$$R_4^+ \otimes R_4^+ \otimes \Gamma_1^+ = \Gamma_1^+ + \Gamma_3^+ + \Gamma_4^+ + \Gamma_5^+. \quad (3)$$

The result contains  $\Gamma_1^+$ , the totally symmetric representation of  $Pm\bar{3}m$ , so that the selection rule is fulfilled, allowing the  $R_4^+$  distortion to give rise to an  $R_4^+ - \Gamma_1^+$  interaction. In other words, the  $a^-a^-a^-$ -type ORs are likely to be attributable to the SOJT mechanism. Compatibility relations reveal that the VB and CB extrema of the  $Pm\bar{3}m$  phase respectively split as follows:

$$[R_4^+]_{Pm\bar{3}m} \rightarrow [\Gamma_1^+]_{R\bar{3}c} + [\Gamma_3^+]_{R\bar{3}c}, \quad (4)$$

and

$$[\Gamma_1^+]_{Pm\bar{3}m} \rightarrow [\Gamma_1^+]_{R\bar{3}c}. \quad (5)$$

One can expect that the new bonding and antibonding states belong to the irrep  $[\Gamma_1^+]_{R\bar{3}c}$  and that the  $[\Gamma_3^+]_{R\bar{3}c}$  state remains nonbonding because of the absence of CB states with the same symmetry. Although some X–M interactions couple to the  $R_4^+$  distortion [30], we ignore them because of their large energy gaps.

We next assess the dependence of band-resolved projected crystal orbital Hamiltonian population (COHP) [64–68] between F 2p and Ga 4s states—composing the  $R_4^+$  and  $\Gamma_1^+$  states, respectively [30]—on the rotation magnitude. The rotation distortion is parametrized by reaction coordinate  $\lambda$  varying from 0 (fully relaxed high-symmetry structure) to 1 (fully relaxed low-symmetry structure). We use negative-signed COHPs ( $-\text{COHPs}$ ) whose positive (negative) values represent bonding (antibonding) interactions. Figure 2(c) illustrates that the  $-\text{COHPs}$  for the  $R_4^+$  VB states change significantly with  $\lambda$ . Although there is no bonding interaction for the VB states in the  $Pm\bar{3}m$  configuration ( $\lambda = 0$ ), these states split at finite  $\lambda$ , and the  $-\text{COHP}$  for the  $[\Gamma_1^+]_{R\bar{3}c}$  state increases on approaching  $\lambda = 1$ . This behavior proves that the rotation magnitude strongly correlates with the degree of  $R_4^+ - \Gamma_1^+$  bonding interaction. The  $-\text{COHP}$  for the  $[\Gamma_3^+]_{R\bar{3}c}$  states remains close to zero, supporting the nonbonding nature expected from the above symmetry arguments. By checking a decrease in the  $-\text{COHP}$  with increasing  $\lambda$ , we also validate the antibonding character of  $\Gamma_1^+$  CB state with

which the considered VB states mix [30]. Figure 2(d) plots the  $-\text{COHPs}$  between Ti  $3d-t_{2g}$  and O  $2p$  states for the  $\Gamma_4^-$  VB states of  $\text{BaTiO}_3$  against  $\lambda$ , where the low-symmetry structure corresponds to  $P4mm$  one. Comparing Figs. 2(c) and 2(d) reveals that the evolutions of bonding interactions in  $\text{GaF}_3$  are very similar to those in  $\text{BaTiO}_3$ , implying that  $\text{Ga}(4s)-\text{F}(2p)$  bonding drives the ORs in the same way that  $\text{Ti}(3d)-\text{O}(2p)$  bonding drives the polar displacements in  $\text{BaTiO}_3$ . The difference in behavior between the  $-\text{COHPs}$  of  $\text{GaF}_3$  and  $\text{BaTiO}_3$  when  $\lambda \rightarrow 1$  is discussed in the Supplemental Material [30].

The covalent bonds in  $\text{BaTiO}_3$  cause a shift down (up) in energy of its occupied bonding (unoccupied antibonding) state to produce a net energy gain to the polar phase [69]. Here, we demonstrate that by calculating band dispersions with varying  $\lambda$ , a similar stabilization arises from  $\text{R}_4^+-\Gamma_1^+$  bonding interactions accompanied by the  $a^-a^-a^-$ -type ORs. In the  $R\bar{3}c$  structures where the  $\text{R}_4^+$  VB states split [Eq. (4)], the increase in  $\lambda$  (and therefore in the OR magnitude) lowers the energy of the bonding  $[\Gamma_1^+]_{R\bar{3}c}$  state while keeping that of the nonbonding  $[\Gamma_3^+]_{R\bar{3}c}$  state almost unchanged [Fig. 2(e)]. Also, destabilization of the CB  $\Gamma_1^+$  state in response to the ORs is manifest in Fig. 2(f). Thus, we find that the ORs—unfavorable in terms of Madelung energy—become energetically favorable because of the bonding interaction that stabilizes the electronic system. Although the  $[\Gamma^-]_{Pm\bar{3}m}$  state in Fig. 2(e) shifts upward, the total energy penalty at the  $[\Gamma^-]_{Pm\bar{3}m}$  point is almost zero, not offsetting the energy reduction at the R point [30]. There is no conceptual difference from the polar shifts in  $\text{BaTiO}_3$ , except that for the case of ORs the interacting Bloch states locate at distinct  $k$ -points in the high-symmetry configuration. Note in Fig. 2(e) that the energy of the  $\text{M}_3^+$  VB states is quite insensitive to the  $a^-a^-a^-$ -type ORs, as expected from symmetry considerations [30]. Instead, the increase in the  $a^+a^+a^+$ -type rotation in magnitude lowers the energy of the  $\text{M}_3^+$  state but does not influence the  $\text{R}_4^+$  state [30].

Next, we provide a real-space picture of the bond formation in  $\text{GaF}_3$ . The  $Pm\bar{3}m$  configuration having linear Ga–F–Ga chains results in an equal amount of constructive and destructive overlap between the  $\Gamma_1^+$  CB and  $\text{R}_4^+$  VB states; the two are orthogonal [Figs. 3(a) and 3(b)]. When

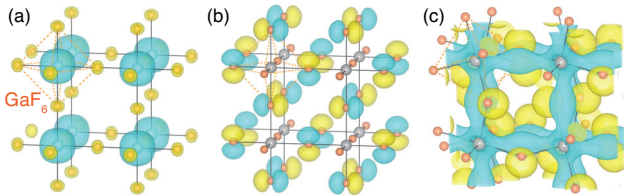


FIG. 3. Real part of the wave functions for (a)  $[\Gamma_1^+]_{Pm\bar{3}m}$  CB and (b)  $[\text{R}_4^+]_{Pm\bar{3}m}$  VB states of the  $Pm\bar{3}m$  structure, and (c)  $[\Gamma_1^+]_{R\bar{3}c}$  VB state of the  $R\bar{3}c$  structure. Yellow (blue) isosurface denotes positive (negative) lobes.

the ORs occur so as to bend Ga–F–Ga angle, however, the two states are no longer orthogonal and can mix to form a low-energy bonding state. Indeed, the  $[\Gamma_1^+]_{R\bar{3}c}$  VB state now exhibits a substantial wave function’s magnitude in an area between the Ga and F sites [Fig. 3(c)]. This  $sp\pi$  bonding is reminiscent of the  $dp\pi$  and  $dp\sigma$  bondings of  $\text{BaTiO}_3$  [18,70]. One might expect anion–anion bonds to stabilize the tilted structure because such a stabilization mechanism is well established in skutterudites such as  $\text{RhP}_3$  [71–73], whereas both the F–F bonding and antibonding states appear below the Fermi energy and offer no net stabilizing effect [Fig. 4(a)]. This is in striking contrast to P–P bonds [Fig. 4(b)], i.e.,  $\text{P}_4$  polyanionic rings in  $\text{RhP}_3$  due to which the  $Im\bar{3}$  structure is substantially lower in energy relative to  $R\bar{3}c$  and  $Pm\bar{3}m$  phases (Supplemental Material [30]).

Both  $\text{RhF}_3$  and  $\text{AlH}_3$  crystallize in  $R\bar{3}c$  structures [74,75], where band dispersions near the Fermi levels (and hence the symmetry of wave functions) are considerably different from those of  $\text{GaF}_3$ . The CB of  $\text{RhF}_3$  consists mainly of  $4d$  rather than  $4s$  states [Fig. 4(c)], and the VB of  $\text{AlH}_3$  is dominated by H  $1s$  states instead of  $2p$  states of O or F [Fig. 4(d)]. Despite such differences, our direct product calculations prove that the  $\text{R}_4^+$  distortion can be stabilized in  $\text{RhF}_3$  and  $\text{AlH}_3$  by  $\text{R}_5^+-\Gamma_3^+$  and  $\text{R}_4^+-\Gamma_4^-$  bonding, respectively (Supplemental Material [30]). Also in  $\text{ReO}_3$ , the pair of  $\text{R}_5^+$  and  $\Gamma_3^+$  states is symmetry allowed to interact under the distortion and results in bonding and antibonding orbitals. However, both of them are unoccupied, producing no net energy gain [Fig. 4(e)].  $\text{ReO}_3$  is

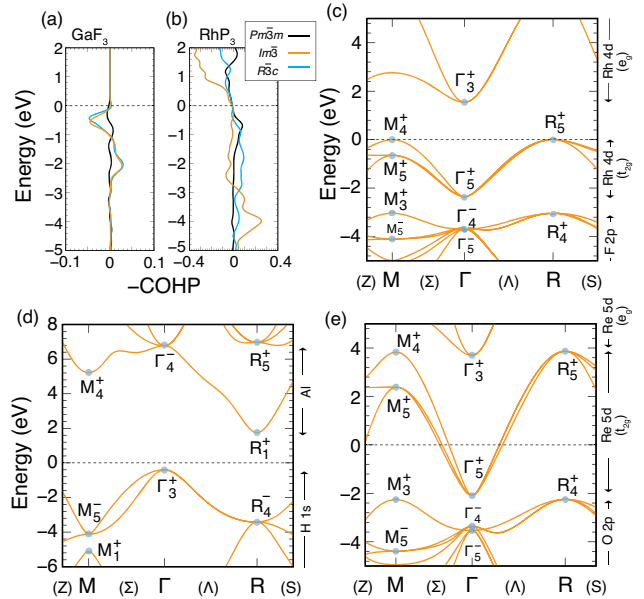


FIG. 4. Averaged  $-\text{COHPs}$  of anion–anion bondings (Supplemental Material [30]) in the  $Pm\bar{3}m$ ,  $R\bar{3}c$ , and  $Im\bar{3}$  structures of (a)  $\text{GaF}_3$  and (b)  $\text{RhP}_3$ . Electronic band structures for (c)  $\text{RhF}_3$ , (d)  $\text{AlH}_3$ , and (e)  $\text{ReO}_3$  with  $Pm\bar{3}m$  structures.

therefore predicted to retain the aristotype  $Pm\bar{3}m$  structure, consistent with experimental reports [76,77].

Generally, more than one pair of Bloch states around the Fermi level interact under a given distortion. For example, in  $\text{ReO}_3$ ,  $R_4^+$  displacive perturbation permits  $R_4^+-\Gamma_3^+$  and  $R_4^+-\Gamma_5^+$  interactions as well [30]. Although a stabilizing effect is expected from the former interaction, this would be counteracted by an energy penalty due to the populated antibonding state arising from the latter. We believe that an orbital- and band-resolved decomposition of the quadratic coefficient of Eq. (1) enables quantitative discussions on such competing effects, which could be accomplished by an extension of the approach developed in Ref. [78]. This may also allow incorporating the effect of hybridization into the tolerance factor approach [79], leading to a new descriptor for the structural instability.

To summarize, we have proposed that the SOJT effect, when combined with the band folding scenario, can uncover the driving mechanism of nonzero- $q$  displacements. Based on this idea, we have demonstrated that energy-lowering  $B-X$  bondings trigger the ORs even with the empty  $A$ -site cavities. As for  $ABX_3$  perovskites [30],  $B-X$  and  $A-X$  bondings will cooperatively induce ORs, though the latter contribution is secondary. Although only zone-boundary distortions are discussed here, the same framework can obviously apply to any distortions including incommensurate modulations. We hope this study leads to a unified description of a variety of structural distortions in solids that will be exploited for rational property design.

This work was supported by Research Fellowships of Japan Society of the Promotion of Science (JSPS) for Young Scientists, the Grant-in-Aid for JSPS Research Fellow (Grant No. JP20J01149), JSPS KAKENHI (Grants No. JP18H01892, No. JP21K19027, No. JP21H05568, and No. JP16H06440), and Murata Science Foundation. The computation was carried out using the computer resource offered under the category of General Projects by Research Institute for Information Technology, Kyushu University.

\*suguru.yoshida0224@gmail.com

- [1] We use the symbols  $q$  and  $k$  to denote wave vectors of phonons (and distortions) and electronic states, respectively.  
 [2] J. Kanamori, *J. Phys. Chem. Solids* **10**, 87 (1959).  
 [3] J. B. Goodenough, *Phys. Rev.* **100**, 564 (1955).  
 [4] T. Goto, T. Kimura, G. Lawes, A. P. Ramirez, and Y. Tokura, *Phys. Rev. Lett.* **92**, 257201 (2004).  
 [5] C. J. Fennie and K. M. Rabe, *Phys. Rev. B* **72**, 100103(R) (2005).  
 [6] H. Akamatsu, K. Fujita, T. Kuge, A. Sen Gupta, A. Togo, S. Lei, F. Xue, G. Stone, J. M. Rondinelli, L.-Q. Chen, I. Tanaka, V. Gopalan, and K. Tanaka, *Phys. Rev. Lett.* **112**, 187602 (2014).  
 [7] X.-Z. Lu and J. M. Rondinelli, *MRS Adv.* **5**, 3521 (2020).

- [8] J. S. O. Evans, T. A. Mary, T. Vogt, M. A. Subramanian, and A. W. Sleight, *Chem. Mater.* **8**, 2809 (1996).  
 [9] M. S. Senn, A. Bombardi, C. A. Murray, C. Vecchini, A. Scherillo, X. Luo, and S. W. Cheong, *Phys. Rev. Lett.* **114**, 035701 (2015).  
 [10] T. A. Bird, J. Woodland-Scott, L. Hu, M. T. Wharmby, J. Chen, A. L. Goodwin, and M. S. Senn, *Phys. Rev. B* **101**, 064306 (2020).  
 [11] A. Ferretti, D. B. Rogers, and J. B. Goodenough, *J. Phys. Chem. Solids* **26**, 2007 (1965).  
 [12] W. Lu, W. Song, P. Yang, J. Ding, G. M. Chow, and J. Chen, *Sci. Rep.* **5**, 10245 (2015).  
 [13] K. Hanzawa, S. Iimura, H. Hiramatsu, and H. Hosono, *J. Am. Chem. Soc.* **141**, 5343 (2019).  
 [14] V. Gopalan and D. B. Litvin, *Nat. Mater.* **10**, 376 (2011).  
 [15] N. A. Benedek and C. J. Fennie, *Phys. Rev. Lett.* **106**, 107204 (2011).  
 [16] M. J. Pitcher, P. Mandal, M. S. Dyer, J. Alaria, P. Borisov, H. Niu, J. B. Claridge, and M. J. Rosseinsky, *Science* **347**, 420 (2015).  
 [17] I. B. Bersuker, *Phys. Lett.* **20**, 589 (1966).  
 [18] R. E. Cohen, *Nature (London)* **358**, 136 (1992).  
 [19] A. Walsh, D. J. Payne, R. G. Egdell, and G. W. Watson, *Chem. Soc. Rev.* **40**, 4455 (2011).  
 [20] N. A. Benedek and C. J. Fennie, *J. Phys. Chem. C* **117**, 13339 (2013).  
 [21] One of the exceptions is Peierls transition, where a one-dimensional crystal with Fermi wave vector  $k_F$  undergoes a distortion with  $q = 2k_F$ .  
 [22] P. M. Woodward, *Acta Crystallogr. Sect. B* **53**, 44 (1997).  
 [23] A. Hampel, J. Lee-Hand, A. Georges, and C. E. Dreyer, *Phys. Rev. B* **104**, 035102 (2021).  
 [24] We follow the terminology in the community of ferroics and use the term “second-order” rather than “pseudo”.  
 [25] I. B. B. V. Z. Polinger, *Vibronic Interactions in Molecules and Crystals*, 1st ed. (Springer-Verlag, Berlin Heidelberg, 1989).  
 [26] I. B. Bersuker, *Chem. Rev.* **113**, 1351 (2013).  
 [27] I. B. Bersuker, B. G. Vekhter, and A. A. Muzalevskii, *Ferroelectrics* **6**, 197 (1973).  
 [28] P. Garcia-Fernandez, J. Aramburu, M. Barriuso, and M. Moreno, *J. Phys. Chem. Lett.* **1**, 647 (2010).  
 [29] H. Mizoguchi, P. M. Woodward, S.-H. Byeon, and J. B. Parise, *J. Am. Chem. Soc.* **126**, 3175 (2004).  
 [30] See Supplemental Material at <http://link.aps.org/supplemental/10.1103/PhysRevLett.127.215701> for computational details, notes for the SOJT effect, the difference between -COHPs of  $\text{GaF}_3$  and  $\text{BaTiO}_3$ , and the energy penalty at the  $\Gamma$  point, discussions on the in-phase  $M_3^+$  rotation and perovskite compounds, results of the density of state calculations, and additional direct product calculations, which includes Refs. [31–47].  
 [31] H. J. Monkhorst and J. D. Pack, *Phys. Rev. B* **13**, 5188 (1976).  
 [32] B. J. Campbell, H. T. Stokes, D. E. Tanner, and D. M. Hatch, *J. Appl. Crystallogr.* **39**, 607 (2006).  
 [33] K. Momma and F. Izumi, *J. Appl. Crystallogr.* **44**, 1272 (2011).  
 [34] Y. Hinuma, G. Pizzi, Y. Kumagai, F. Oba, and I. Tanaka, *Comput. Mater. Sci.* **128**, 140 (2017).

- [35] A. M. Ganose, A. J. Jackson, and D. O. Scanlon, *J. Open Source Softw.* **3**, 717 (2018).
- [36] T. B. Boykin and G. Klimeck, *Phys. Rev. B* **71**, 115215 (2005).
- [37] W. Ku, T. Berlijn, and C.-C. Lee, *Phys. Rev. Lett.* **104**, 216401 (2010).
- [38] P. B. Allen, T. Berlijn, D. A. Casavant, and J. M. Soler, *Phys. Rev. B* **87**, 085322 (2013).
- [39] U. Herath, P. Tavazde, X. He, E. Bousquet, S. Singh, F. Muñoz, and A. H. Romero, *Comput. Phys. Commun.* **251**, 107080 (2020).
- [40] V. Wang, N. Xu, J. C. Liu, G. Tang, and W.-T. Geng, *Comput. Phys. Commun.* **267**, 108033 (2021).
- [41] Z. Wang, J. Xi, J. Ning, K. Guo, B. Duan, J. Luo, G. J. Snyder, J. Yang, and W. Zhang, *Chem. Mater.* **33**, 1046 (2021).
- [42] J. Gao, Q. Wu, C. Persson, and Z. Wang, *Comput. Phys. Commun.* **261**, 107760 (2021).
- [43] J. L. Birman, *Phys. Rev.* **125**, 1959 (1962).
- [44] J. L. Birman, *Phys. Rev.* **127**, 1093 (1962).
- [45] M. I. Aroyo, A. Kirov, C. Capillas, J. M. Perez-Mato, and H. Wondratschek, *Acta Crystallogr. Sect. A* **62**, 115 (2006).
- [46] X.-G. Zhao, Z. Wang, O. I. Malyi, and A. Zunger, arXiv: 2104.09361.
- [47] Y. Mochizuki, H.-J. Sung, A. Takahashi, Y. Kumagai, and F. Oba, *Phys. Rev. Mater.* **4**, 044601 (2020).
- [48] *Physics of Ferroelectrics: A Modern Perspective*, edited by K. M. Rabe, C. H. Ahn, and J.-M. Triscone, Topics in Applied Physics (Springer-Verlag, Berlin Heidelberg, 2007).
- [49] J. M. Rondinelli, A. S. Eidelson, and N. A. Spaldin, *Phys. Rev. B* **79**, 205119 (2009).
- [50] L. D. Landau and L. M. Lifshitz, *Quantum Mechanics: Non-Relativistic Theory*, 3rd ed. (Butterworth-Heinemann, Singapore, 1981).
- [51] M. S. Dresselhaus, G. Dresselhaus, and A. Jorio, *Group Theory: Application to the Physics of Condensed Matter* (Springer-Verlag, Berlin Heidelberg, 2008).
- [52] To prevent ambiguity, we sometimes use the subscript symbol denoting the space group with respect to which the irrep is defined.
- [53] A. M. Glazer, *Acta Crystallogr. Sect. B* **28**, 3384 (1972).
- [54] P. E. Blöchl, *Phys. Rev. B* **50**, 17953 (1994).
- [55] G. Kresse and D. Joubert, *Phys. Rev. B* **59**, 1758 (1999).
- [56] J. Heyd, G. E. Scuseria, and M. Ernzerhof, *J. Chem. Phys.* **118**, 8207 (2003).
- [57] J. Heyd, G. E. Scuseria, and M. Ernzerhof, *J. Chem. Phys.* **124**, 219906 (2006).
- [58] A. V. Krukau, O. A. Vydrov, A. F. Izmaylov, and G. E. Scuseria, *J. Chem. Phys.* **125**, 224106 (2006).
- [59] G. Kresse and J. Hafner, *Phys. Rev. B* **47**, 558 (1993).
- [60] G. Kresse and J. Hafner, *Phys. Rev. B* **48**, 13115 (1993).
- [61] G. Kresse and J. Furthmüller, *Phys. Rev. B* **54**, 11169 (1996).
- [62] G. Kresse and J. Furthmüller, *Comput. Mater. Sci.* **6**, 15 (1996).
- [63] M. Roosand and G. Meyer, *Z. Kristallogr.* **216**, 18 (2001).
- [64] R. Dronskowski and P. E. Bloechl, *J. Phys. Chem.* **97**, 8617 (1993).
- [65] V. L. Deringer, A. L. Tchougréeff, and R. Dronskowski, *J. Phys. Chem. A* **115**, 5461 (2011).
- [66] S. Maintz, V. L. Deringer, A. L. Tchougréeff, and R. Dronskowski, *J. Comput. Chem.* **34**, 2557 (2013).
- [67] X. Sun, X. Li, J. Yang, J. Xi, R. Nelson, C. Ertural, R. Dronskowski, W. Liu, G. J. Snyder, and D. J. Singh, *J. Comput. Chem.* **40**, 1693 (2019).
- [68] R. Nelson, C. Ertural, J. George, V. L. Deringer, G. Hautier, and R. Dronskowski, *J. Comput. Chem.* **41**, 1931 (2020).
- [69] A. Filippetti and N. A. Hill, *Phys. Rev. B* **65**, 195120 (2002).
- [70] D. Hickox-Young, D. Puggioni, and J. M. Rondinelli, *Phys. Rev. B* **102**, 014108 (2020).
- [71] I. Lefebvre-Devos, M. Lassalle, X. Wallart, J. Olivier-Fourcade, L. Monconduit, and J. C. Jumas, *Phys. Rev. B* **63**, 125110 (2001).
- [72] H. Luo, J. W. Krizan, L. Muechler, N. Haldolaarachchige, T. Klimczuk, W. Xie, M. K. Fuccillo, C. Felser, and R. J. Cava, *Nat. Commun.* **6**, 1 (2015).
- [73] R. Hanus, X. Guo, Y. Tang, G. Li, G. J. Snyder, and W. G. Zeier, *Chem. Mater.* **29**, 1156 (2017).
- [74] L. Grosse and R. Hoppe, *Z. Anorg. Allg. Chem.* **552**, 123 (1987).
- [75] J. W. Turley and H. W. Rinn, *Inorg. Chem.* **8**, 18 (1969).
- [76] K. Meisel, *Z. Anorg. Allg. Chem.* **207**, 121 (1932).
- [77] E. S. Božin, T. Chatterji, and S. J. L. Billinge, *Phys. Rev. B* **86**, 094110 (2012).
- [78] P. García-Fernández, J. A. Aramburu, M. Moreno, M. Zlatar, and M. Gruden-Pavlović, *J. Chem. Theory Comput.* **10**, 1824 (2014).
- [79] V. M. Goldschmidt, *Naturwissenschaften* **14**, 477 (1926).